Geoderma 470 (2026) 117838

Contents lists available at ScienceDirect

Geoderma

journal homepage: www.elsevier.com/locate/geoderma

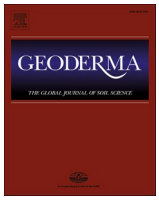

Quantification of field earthworm burrowing rates using repeated X-ray scanning of open soil cores

Rebecca Naomi ter Borg [a,*], Mats Larsbo [a], Yvan Capowiez [b], Pascal Benard [a], Astrid Taylor [c], Daniel Iseskog [a], Thomas Keller [a,d]

[a] Swedish University of Agricultural Sciences, Department of Soil and Environment, Box 7014, 75007 Uppsala, Sweden
[b] INRAE Eco&Sols, INRAE, IRD, CIRAD, Institut Agro Montpellier, Université Montpellier, Montpellier, France
[c] Swedish University of Agricultural Sciences, Department of Ecology, Box 7044, 75007 Uppsala, Sweden
[d] Agroscope, Department of Agroecology and Environment, Reckenholzstrasse 191, 8046 Zürich, Switzerland

ARTICLE INFO

Handling Editor: Dr. H Neely

Keywords:
X-ray computed tomography
Anecic
Endogeic
Bioturbation
Burrow network

ABSTRACT

Earthworms contribute to soil functioning by burrowing through soil, but quantitative knowledge of their burrowing activities and how environmental factors influence it under field conditions is still limited. The objectives of this study were to test a method for quantification of the temporal dynamics of in-situ earthworm burrowing rates, and to investigate links between variations in burrowing rates and soil moisture and temperature. Specially designed perforated cylinders repacked with soil were installed in an arable field with a known earthworm community in Uppsala, Sweden, and repeatedly removed, X-ray scanned, and re-installed, during May-October 2023. Earthworm burrow volumes and characteristics of burrow networks were derived from the X-ray images. Burrows were classified into burrows likely originating from endogeic earthworms (burrow diameter $\leq$ 4 mm) and anecic earthworms ($>$ 4 mm). We tested two methodological approaches, using either new repacked soil after each scan or re-installing the same soil cylinder. We also employed two soil moisture treatments (with and without rainout shelters). In-situ soil moisture and temperature were monitored using sensors. The results showed that burrowing rates in newly repacked soils were higher than in the soil columns with the same soil. Depending on treatment and the time of the year, mean burrowing rates varied between 0.05 and 0.64 cm^3 day^{-1}. On average, we estimated that topsoil turnover rate by earthworm burrowing is about 21–42 years in this field where the earthworm abundance was 81 individuals per m^2. The data from the "same soil" treatment indicates that a steady state in earthworm burrow volume was achieved after five months, indicated by the balance between burrow creation and disappearance. In our study, soil moisture appeared to be a more important driver for earthworm burrowing than soil temperature. We show that about 40% of the earthworm burrow volume was classified as anecic earthworm burrows in the topsoil. We conclude that the proposed method using perforated cylinders with repeated scans is suitable for seasonal monitoring and to quantify earthworm burrowing rates under field conditions.

1. Introduction

Earthworm bioturbation mainly refers to the process of displacing and mixing soil by earthworms as they burrow through soil. Bioturbation influences important soil processes including soil formation, drainage, aeration and nutrient cycling (Lavelle 1988; Blouin et al. 2013; Plaas et al. 2019). The contribution of earthworm bioturbation to soil functioning has been recognized a long time ago (Darwin 1881). While studies on earthworm burrowing and bioturbation rates have been conducted under controlled conditions in 2D terraria (Dittbrenner et al. 2011; Arrázola-Vásquez et al. 2022), mesocosms and soil columns (Jégou et al. 1997; Francis & Fraser 1998; Capowiez et al. 2001; 2015), quantitative data on earthworm burrowing and bioturbation rates in field soils under natural conditions remain scarce, but see e.g. Védère et al. (2025) and Leuther et al. (2023). Hence, it remains elusive to quantitatively link earthworm bioturbation to soil functions and soil health or to predict how changes in land use, soil management or climate impact earthworm bioturbation.

* Corresponding author.
E-mail address: rebecca.naomi.ter.borg@slu.se (R.N. ter Borg).

https://doi.org/10.1016/j.geoderma.2026.117838
Received 14 October 2025; Received in revised form 1 April 2026; Accepted 28 April 2026
Available online 6 May 2026

When earthworms burrow through soil, they create new soil (macro) pores and modify the soil pore network (Ruiz et al. 2023). Earthworm burrowing thus influences soil processes and functions that depend on the properties of the macropore networks, such as water and gas transport and storage, carbon and nutrient cycling, and plant root growth. Knowledge of burrowing rates, i.e. amount of burrowing per unit time, is therefore essential to quantify the contribution of earthworms to these soil processes and soil functions, and to propose or inform simulation models that are however up to now rare in soil biology (Barot et al. 2007). The activities of earthworms vary across soils with different soil texture, organic matter content, pH (Baker & Whitby 2003; Ruiz et al. 2015; Taylor et al. 2019) and bulk density (Capowiez et al. 2021). Furthermore, burrowing rates are affected by soil environmental conditions such as soil moisture and soil temperature (Ruiz et al. 2021; Edwards & Arancon 2022; Gergs et al. 2022) and are hence subjected to seasonal weather variations and long-term climate change (Nordström & Nordstrom 1975; Potvin & Lilleskov 2017; Singh et al. 2019). Soil moisture affects earthworm burrowing because earthworms require a humid tegument to breathe and burrow (Edwards & Arancon 2022) and via its effect on soil mechanical resistance (Ruiz & Or 2018; Arrázola-Vásquez et al. 2022). In the long-term, soil conditions can have an indirect impact on earthworm communities (Bardgett & van der Putten 2014; Phillips et al. 2019). Earthworm activity is affected by temperature but earthworms have been found to be active at temperatures as low as around 2 °C (Singh et al. 2019). In temperate climate, soil moisture and soil temperature are usually inversely related. High temperatures and low soil moisture pose a greater limitation to earthworm burrowing than low temperatures and high soil moisture (Nordstrom & Rundgren 1973; Edwards & Arancon 2022). However, in cold climates, such as Scandinavia, low temperatures and soil freezing restrict earthworm burrowing during winter. Optimal and limiting soil moisture and temperature ranges vary between different earthworm species (Edwards & Arancon 2022). When the soil moisture or temperature is unsuitable, earthworms may migrate to more hospitable conditions, such as greater soil depths where the soil is cooler during summer and warmer during winter (Lavelle 1988). Earthworms may also enter diapause, usually referred to as aestivation, to endure unsuitable soil conditions (Nordström & Nordstrom 1975; Lavelle 1988; Eggleton et al. 2009; Holmstrup et al. 2016). To estimate seasonal variations and to quantify annual earthworm burrowing, it is necessary to understand the relationship between burrowing activity and environmental conditions.

Knowledge of earthworm burrowing rates under field conditions is limited. So far, most experimental studies addressing earthworm burrowing have been conducted under semi-field conditions using cylinders with a certain number of earthworms (i.e., earthworms were enclosed in a confined soil volume) that were placed in the field (Francis & Fraser 1998) or under laboratory settings at temperature ranges of 12–20 °C (Jégou et al. 1997; Capowiez et al. 2011; 2015; Heinze et al. 2021). Earthworm bioturbation rates have also been estimated based on field-sampled earthworm biomass, laboratory-determined egestion rates and mean annual temperature (Taylor et al. 2019; Torppa & Taylor 2022). Recently, Védère et al. (2025) quantified the formation of biopores from soil macrofauna (including earthworms) by in-situ incubation of soil cores in perforated cylinders. However, these studies did not focus on the temporal dynamics but quantified volumes and characteristics of burrows after a given time.

Garbout et al. (2013), Koestel & Schlüter (2019), and Leuther et al. (2023) quantified changes in soil structure and soil pore characteristics by repeated X-ray computed tomography scanning of soil columns installed in the field. Perforated cylinders allow macrofauna to enter and leave the soil cores (Leuther et al. 2023; Schefer et al. 2025; Védère et al. 2025). In this way and by using specific markers, Leuther et al. (2023) identified macrofaunal activity as the main driver for soil structure turnover. They also showed that bioturbation was limited under dry conditions. However, Leuther et al. (2023) did not quantify earthworm burrowing rates. Védère et al. (2025) reported that biopores are typically regenerated (i.e., a steady-state situation is reached) within a year. Moreover, they found that biopores created by earthworms had specific characteristics that allowed distinction from biopores associated with other macrofauna. Earthworms are often classified into three ecological categories, (epigeic, endogeic and anecic), although recent research proposed that species typically have traits of multiple categories and that species may also adjust their burrowing and feeding behaviour to site-specific conditions (Bottinelli et al. 2020; Capowiez et al. 2024). Epigeic earthworms live and feed mainly in the litter layer on the soil surface and are rare or absent in arable soils. Endogeic earthworms feed on soil organic matter and typically create non-directional burrows mainly in the topsoil. Anecic earthworms, also called “deep burrowers”, create and live in deep permanent vertical burrows and feed mainly on litter on the soil surface (Bouché 1977). Burrowing rates vary between different species of earthworms, and the impact of soil environmental conditions on these rates should, therefore, be species dependent. This implies that temporal burrowing patterns vary across species and ecological categories.

Here, we present a method for monitoring changes in earthworm burrow networks in field soil using repeated X-ray tomography scanning of perforated soil cylinders. We installed soil cylinders in an arable field under ley and quantified burrow characteristics and burrowing rates during a five-months period. In line with suggestions from Védère et al. (2025), we aimed at scanning at relatively high temporal resolution (approximately every 1.5–2 months) to capture temporal dynamics in burrowing rates. Given the novelty of this temporal resolution and the associated uncertainty regarding whether earthworm burrow dynamics can be reliably captured at such intervals, we compared two methodological approaches. We either reinstalled the same soil columns after each scan (i.e., without disturbing the soil core) or used newly repacked soil columns after each scan (i.e., installing freshly remoulded soil columns after each measurement). Each of these methods has advantages and disadvantages. For example, re-using the same soil requires image alignment, which can be challenging, but allows quantification of burrow persistence. We also expected that the two methods would provide indications of earthworm behaviour regarding colonizing “new” soil versus re-using existing burrows. We installed in-situ soil sensors to be able to quantify effects of soil moisture on burrowing rates. Finally, we differentiated between anecic and endogeic burrows to characterize different aspects of the burrow systems.

2. Materials and methods

2.1. Experimental design

This study was designed to quantify earthworm burrowing over the course of five months (May – October 2023), based on repeated X-ray tomography scanning of soil columns at 1.5–2 months intervals. Guided by previous work (Leuther et al., 2023), we designed perforated cylinders that allowed earthworms to enter from the sides, the top and bottom (Fig. 1A and Supplementary Fig. S1). The cylinders were designed to maximize the area through which earthworms could enter and exit the soil. Cylinders should also be easy to handle during installation in the field, transport and reinstallation. Moreover, we designed cylinders that can be 3D-printed. Finally, the cylinder dimensions should physically fit into the available X-ray scanner and allow for sufficient image resolution. The cylinders were 20 cm high with a diameter of 10 cm. On the sides, top and bottom of the cylinders, 244 holes with a diameter of 11 mm were evenly distributed, (Fig. 1A). In total, 32 cylinders were 3-D printed with X-PLA material (Add:North 3D-filament).

The field experiment was conducted in 2023 at an arable field under ley (a mixture of grasses and legumes) at Lövsta (59°49′49.9″N 17°48′35.8″E, WGS84), 10 km east of Uppsala, Sweden. The topsoil texture was classified as silty clay (54.1% clay, 41.7% silt and 4.2% sand). The pH of the soil was 6.6 and the organic carbon content was 4.1%. The field was converted to organic farming in 2022, and arable

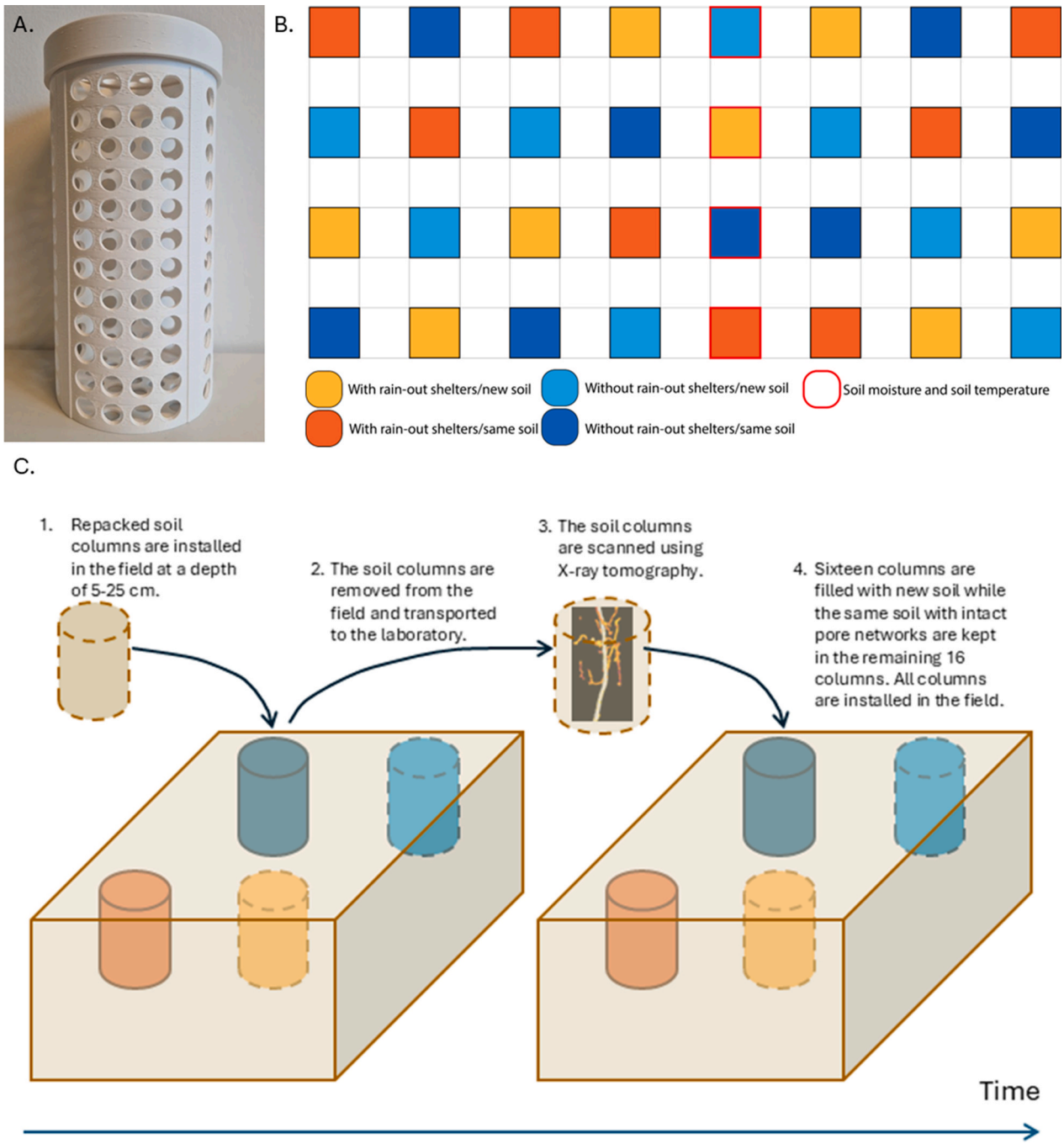

Fig. 1. Design of the cylinders and setup of the experiment. A) Perforated X-PLA cylinder with a height of 20 cm and a diameter of 10 cm. B) Experimental setup in the field with the location of each cylinder. Squares were 1 m x 1 m, the cylinders were placed at the centre of the squares, and there were 2 m between cylinders. The soil moisture and soil temperature sensors were placed inside the cylinders of the 5th column. C) Procedure for installing and removing soil columns from the field. Columns were installed at 5–25 cm depth, with a 5 cm layer of soil placed above them. Steps 2, 3 and 4 were repeated in July and September, in October, only steps 2 and 3 were taken after which the experiment was terminated.

crops are rotated with ley. The preceding crop in 2022 was spring wheat. Five earthworm species were found in the field (a detailed description of earthworm sampling is provided further below, and results are listed in Table S2): *Aporrectodea rosea, Aporrectodea caliginosa, Aporrectodea tuberculata, Aporrectodea longa* and *Lumbricus terrestris*.

We collected soil from the top 30 cm in April 2023. The soil was air-dried and sieved through a 2-mm mesh to remove large plant residues, macrofauna and a negligible amount of gravel. Before packing the soil into cylinders, the gravimetric water content was adjusted to 0.3 kg kg^{-1} (similar to field conditions) and allowed to equilibrate for approximately 48 h. Each cylinder was carefully packed, layer by layer, to a soil bulk density of 1,100 kg m^{-3}, consistent with field observations. Each layer was approximately 2 cm thick, and a total of ten layers were added. No earthworms or additional organic matter were added to the soil to ensure conditions similar to the surrounding soil.

The soil columns were installed in the field on the 25th of May 2023 at a depth of 5–25 cm. First, the top 5 cm of soil and the vegetation were removed, and a hole with a diameter of approximately 14 cm was drilled for each soil column. After placing the soil columns in the hole, soil was filled into the gaps between walls of the hole and the cylinder and

compacted to a similar bulk density as the surrounding soil. The 5 cm of soil and vegetation were placed back on top of the soil columns.

The field experiment was designed with two soil environmental treatments and two method treatments. The two environmental treatments aimed to create "dry" and "wet" soil conditions. For the dry treatment, rainout shelters were placed over the soil columns to intercept any rain on days when forecasted precipitation exceeded 5 mm day^{-1} between 1st of August until 30th of October. For the wet treatment, the soil columns remained uncovered. The environmental treatments are hereafter referred to as "with rainout shelter" and "without rainout shelter". As we will see later, the rainout shelters did not have the intended effect on soil moisture. To test the methodological approach, two treatments were applied: we either re-installed the same soil columns with intact burrow networks after each scan (hereafter referred to as "same soil"; 16 out of 32 columns) or installed freshly remoulded, repacked soil after each scan (referred to as "new soil"; remaining 16 columns). Each of the four-treatment combination (i.e. same soil with rainout shelter, same soil without rainout shelter, new soil with rainout shelter, new soil without rainout shelter) had thus eight replicates, which were arranged in eight blocks (Fig. 1B). One cylinder of the treatment combination "with rainout shelter" and "same soil" broke in the field, resulting in only seven replicates for this treatment combination. In-situ soil water content (volumetric water content in m^3 m^{-3}) and soil temperature (°C) were monitored with four "GS3 sensors" (METER Group, München, Germany) that were inserted into the centre of one soil column per treatment (Fig. 1B). The calibration of the soil moisture readings was based on the protocol provided by METER Group (München, Germany), and calibration results are given in supplementary materials: Calibration of in-situ soil moisture sensors and the sensor data through the season in supplementary figure S4.

Soil columns were removed from the field, X-ray scanned and re-installed on three occasions during the growing season 2023 (Fig. 1C): 24 July (day 60 after initial installation), 11 September (day 109) and 30 October (day 158). To avoid any disturbance during transportation, soil columns were placed in padded boxes with filling material. Period 1 (25 May – 24 July) was characterised by limited precipitation (May – June: 3 mm and July: 69 mm) and a mean air temperature of 16.6 °C, period 2 (24 July – 11 September) was characterized by normal (i.e., similar to the long-term mean) precipitation (137 mm) and a mean air temperature of 15.9 °C, and period 3 (11 September – 30 October) was characterized by normal precipitation (57 mm) and an average air temperature of 8.1 °C (Supplementary Table S1 and Supplementary Fig. S2). In July, the experimental area was mowed using a hand mower and the grass was removed.

On the 3rd November 2023, i.e. four days after removing the soil columns, earthworms were collected to determine earthworm abundance, fresh biomass, and species. We collected earthworms along a transect at the outer perimeter of the installed cylinders, and hand sorted earthworms from four dug holes of 40 cm × 40 cm × 40 cm. The sampling was repeated in October 2024.

2.2. X-ray computed tomography scanning, image processing and image analysis

2.2.1. X-ray tomography scanning and image processing using ImageJ

Soil columns were scanned with a GE *Phoenix* (V|tome|x 240) X-ray tomograph at the Department of Soil and Environment at the Swedish University of Agricultural Sciences in Uppsala. For each soil column, 2000 radiographs were taken at a voltage of 170 kV, a current of 630 μA and an exposure time of 200 ms. Three-dimensional images were reconstructed with *Dragon*fly 3D World, version 2024.1.0.1601. The resulting voxel edge length was 120 μm.

Image J and plugins in the Fiji distribution were used for image processing (Schindelin et al. 2012). Fig. 2 visualizes the steps to obtain an image of the burrow network. As part of the preprocessing, grey values were calibrated for each soil column to standardize the grey-scale

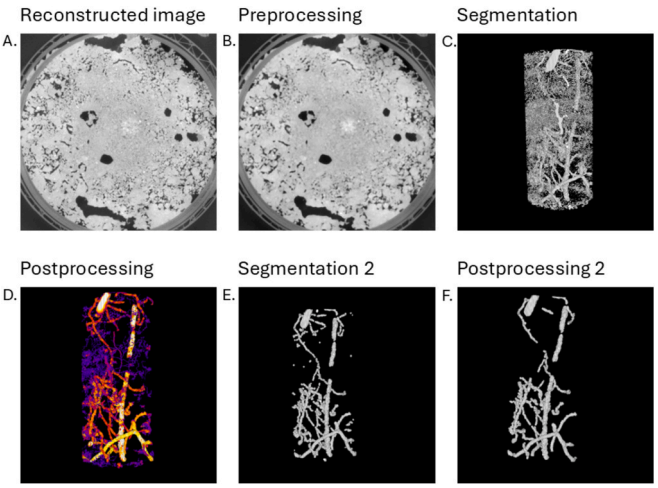

Fig. 2. Visualization of the processing steps to extract the burrow network. A) Reconstructed image after grey scale calibration, B) preprocessing to reduce noise, C) segmentation to determine the pore network, D) postprocessing to further remove noise by filling holes, merging pores and removing singular voxels and small clusters of voxels (colours indicate the diameter of the pores), E) second segmentation for removal of pores with diameters smaller than 2 mm, and F) postprocessing step no 2 to obtain final burrow network, where small clusters of voxels were removed.

distribution in the images. To reduce noise, a 3D median filter with a radius of three voxels was applied. For each cylinder, a representative volume (1550 slices) was extracted from the centre of the cylinders to be able to compare burrow networks across samples. The images were segmented using the Otsu method. The segmented images were processed in three steps to fill holes, merge groups of voxels that are next to each other, and remove noise, and we used the following commands: 3D fill holes (Ollion et al. 2013); erode and dilate; and size opening 2D/3D (Legland et al. 2016). The local thickness command (Dougherty & Kunzelmann 2007) was used to calculate the pore diameter, and pores with thicknesses smaller than 2 mm were removed. Earthworm burrow diameter differs between species and stage of development and generally ranges from 1-12 mm (Edwards & Arancon 2022). We used 2 mm as a cut-off to exclude biopores created by roots and smaller soil fauna (with a risk of potentially excluding burrows created by small earthworms). Finally, after visual inspection of the original X-ray images, remaining solitary pores that were most likely not earthworm burrows were removed using size opening 2D/3D (Ollion et al. 2013) with a minimum voxel count of 50000.

Earthworm casts could not be extracted from the X-ray images because grey values were similar to those of soil. Earthworms were present in some of the soil columns when they were scanned. They were digitally removed from the images using the morphological segmentation implemented in the MorphoLibJ (Legland et al. 2016) plugin with an approach previously used to segment earthworm casts (Arrázola-Vásquez et al., 2024). The tolerance intensity parameter was set to 1500 (−), but in some cases, tolerance values of 1800 or 2000 were used for a better segmentation quality. The resulting segmented catchment image is an image that contains "catchments" that are the different groups of grey values. This image was entered in the label edition where catchments containing earthworm were manually labelled and removed from the images. To transform the label edition image to a binary image, the catchment image was first dilated once, to connect the separate catchments, after which it was converted to a binary image The same postprocessing steps as for the pores were used (Supplementary figure S4). The pore images and earthworm images were then combined to generate a final image of the pore network created by earthworms.

2.2.2. Image processing using Matlab

Binary images of segmented macropores of "same soil" cylinders were aligned in a three-step procedure using MATLAB (The MathWorks Inc. 2024). First, the initial binarized volume was rotated to minimize its difference with the following scan using the inbuilt functions 'imrotate' and 'imrotate3'. Second, differences between initial rotated volume and following binarized original volume were further minimized by shifting the initial volume in x ,y and z direction, i.e. performing a translation transformation of the initial rotated volume using the inbuilt functions 'imregtform' and 'imwarp'. Third, to account for differences in burrow alignment caused by slight sample tilt, mismatches caused by limited spatial resolution, and swelling and shrinking of soil and burrows induced by gradients in soil moisture, an elastic alignment of image slices from top to bottom was performed. In this process, the first slice where an overlap of pores occurred between the initial, rotated and shifted binarized volume and the following binarized volume was shifted in x and y direction using the inbuilt functions 'imregtform' and 'imwarp' to minimize the difference between binary images and to create a starting point for further alignment. Shifts of following slices in the z-direction to minimize differences between binarized volumes were restricted to one pixel in the x- and y-directions. Visual inspection showed highly aligned burrows.

2.2.3. Burrow volume and rates of burrow creation and disappearance

For the repacked soil columns with new soil, the Pore Space Analyzer of the SoilJ plugin (Koestel 2018) in ImageJ was used to extract burrow volume and mean burrow thickness, and to create local thickness images. The porosity of each slice was extracted to determine the depth distribution of burrows.

In Matlab, from the aligned images of the "same soil" columns, the total burrow volume was determined at each scan time, and the maintained, newly created and disappeared burrow volume between the first and second, and second and third scan, were calculated. The burrowing rate (cm^3 day^{-1}) and the burrow disappearing rate (cm^3 day^{-1}) were calculated as the pore volume created and disappeared, respectively, divided by the number of days between the scans. The disappearing rate and the maintained burrows are based on individual burrows within a soil column, i.e. accounts for specific burrows that disappeared or were still present, respectively, between scans. We also calculated burrowing rates per volume of soil and day (cm^3 cm^{-3} day^{-1}) (Supplementary Tables S5 and S6). The net burrowing rate for the "same soil" columns was calculated by subtracting the created from the disappeared burrowing rate.

Although we could not assign individual earthworm burrows to specific earthworm species, it is possible to distinguish burrows likely created by endogeic and anecic earthworms, respectively, based on burrow diameter. Based on literature data on earthworm diameters of endogeic and anecic earthworms (Sherlock 2012; Edwards & Arancon 2022) and the anecic earthworms observed in the field, we chose a threshold of 4 mm to separate endogeic and anecic earthworm burrows. We also calculated the fraction of disappeared anecic and endogeic burrows for the "same soil" cylinders and determined burrow persistency defined as the fraction of burrows that disappeared between the first and second scan, and the second and third scan.

Finally, we quantified the orientation, branching and tortuosity of "anecic burrows" and "endogeic burrows". For this, the skeleton of the pore network was obtained using Matlab. All dead-end branches shorter than 1 mm were removed. The binary images were first downscaled to 0.125, which reduced artifacts in the resulting skeletons and in the analysis of skeletons. The skeletons were analysed using the ImageJ plugin Analyze Skeleton (Arganda-Carreras et al. 2010). From this, we received the number of clusters, branches, junctions and endpoints for each pore cluster. Clusters with total branch length smaller than 40 mm were not included in the analysis since they often contained skeletonization artefacts. We also retrieved information on the length of each branch and the coordinates for the endpoints of each branch. From these parameters, we calculated the tortuosity by dividing the branch length by the Euclidean distance between the endpoints. The preferred orientation of burrows was estimated by the angular deviation from the vertical direction (Capowiez et al., 2015). For burrow clusters, we calculated two measures of complexity, the branching intensity (Capowiez et al., 2015), which is the number of junctions per branch length unit, and the coordination number. The coordination number reflects how connected the burrow network is. For all these measures, we first calculated the sum of the parameters included in the measures for each image and then calculated the measures from these sums, thereby giving weight according to the length of each branch or the size of each cluster. These measures were calculated for all "new soil" images and for the last period for the "same soil" images.

2.3. Statistical analysis

The R software version 4.4.2 (R Core Team 2024) was used for all statistical analysis. Graphs were created using the base plot command in the R software and the R packages ggplot2 (Wickham 2016) and ggpubr (Kassambara 2023). To analyse the results, a generalized linear model based on a Tweedie distribution was used (Dunn 2022). The response variable was the burrowing rate and the predictor variables considered were treatments (i.e. "new soil", "same soil", "with rainout shelters" and "without rainout shelters"), block and time of the scanning. Tortuosity, angle, orientation of the burrows, number of clusters, coordination number and branching intensity between anecic and endogeic burrow networks were statistically tested with a linear regression model including block as an additional factor.

3. Results

Illustrations of earthworm burrow networks are shown in Fig. 3. Earthworms entered and exited the soil columns through the perforated cylinder walls from all sides. Repeated X-ray imaging enabled us to

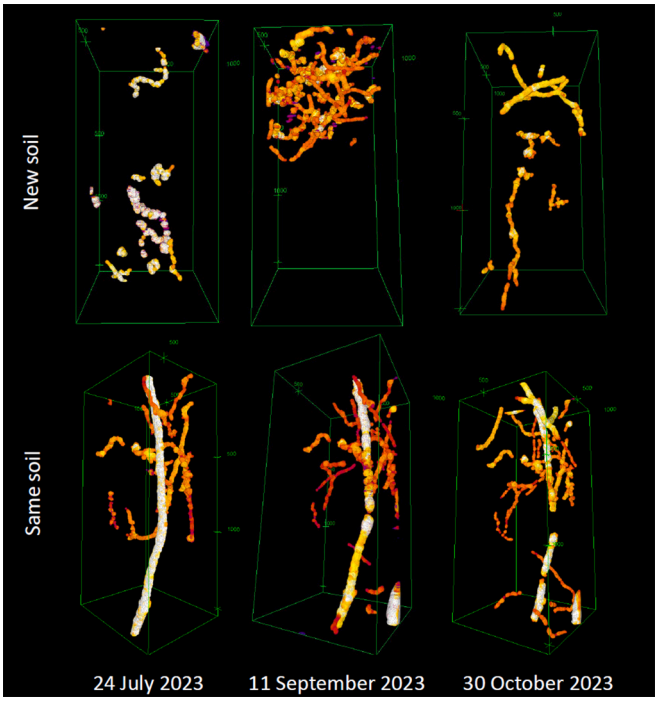

Fig. 3. Illustrative examples of the temporal evolution of earthworm burrow networks derived from X-ray imaging of (top) a cylinder with new repacked soil, and (bottom) a cylinder where the same soil with intact burrow network had been reinstalled in the field. The colours in the images indicate burrow diameters, where white is the largest and orange the smallest diameter; note that the colour scale is relative for each image.

monitor the temporal evolution of earthworm burrow networks in the two different treatments "new" and "same" soil (Fig. 3 top and bottom, respectively). and compare burrows in "repacked" cylinders with those created in "same soil" (Fig. 3). Reinstalling the same soil with intact burrow networks after each X-ray scan enabled us to analyse the appearance and disappearance of burrows between scans, i.e., newly formed and collapsed/refilled burrows (Fig. 2, bottom). Using cylinders with new soil that is repacked after each X-ray scan (Fig. 2, top) facilitated the quantification of the newly created burrow volume between scanning timepoints since the initial conditions (i.e., when installing the soil column in the field) was standardized as "new" soil cores without burrows.

3.1. *Temporal evolution of earthworm burrow volumes and burrowing rates*

The temporal evolution of earthworm burrow networks for all soil columns is presented in Supplementary Fig. S5, and data on created and disappeared burrow volumes and (net) changes in burrow volumes between scans are given in Supplementary Tables S3 and S4. There was variation between burrow volumes in the soil columns of the same treatments, which was visible in the images of the burrow networks (Supplementary Fig. S5) and the extracted burrow volumes (Supplementary Table S3-S6). Fig. 4 shows the calculated rates of burrow volume change and rates of created and disappeared burrow volumes. Note that for the "new soil" cylinders (Fig. 4A), the new burrow volume equals the net change in burrow volume between scans since the columns did not contain any burrows at the start of each period. This was also the case for period 1 for the "same soil" cylinders that started with a repacked soil (Fig. 4B).

Burrowing rates were between 0.05 and 0.2 cm^3 d^{-1} in the "same soil" columns and between 0.05 and 0.7 cm^3 d^{-1} in the "new soil" columns (Fig. 4). Burrowing rates in "new soil" columns were highest during period 2 (25. July – 11. September), while burrowing rates in the

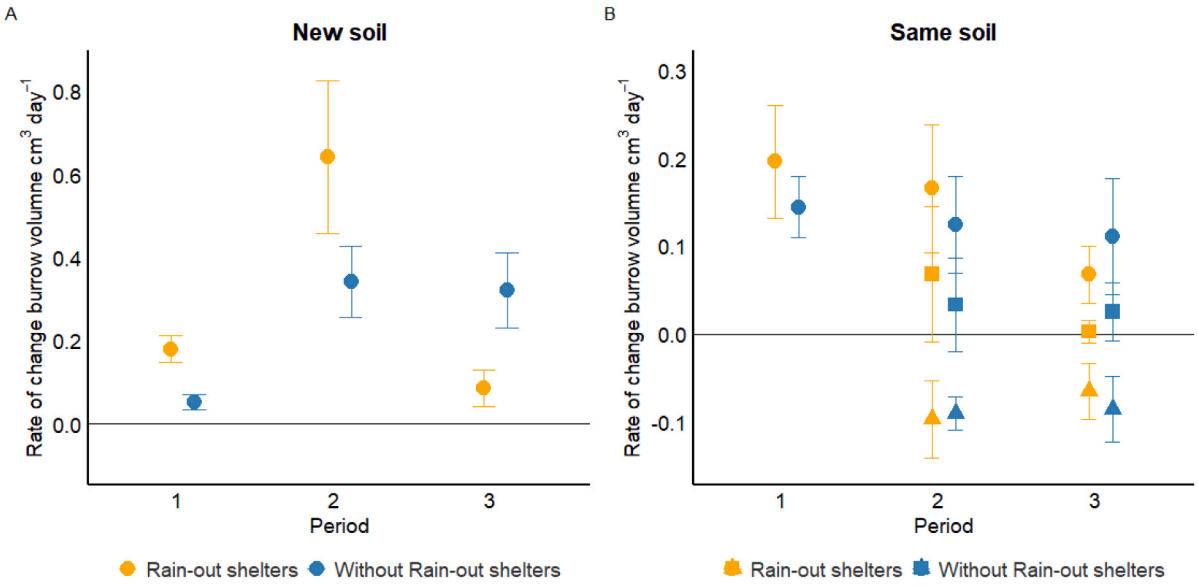

Fig. 4. Rates of change in burrow volume for A) cylinders with repacked new soil after each X-ray scan and B) cylinders where the same soil with intact burrow networks were reinstalled after each X-ray scan. The symbols denote burrowing (circles), disappearance (plotted as negative values; triangles), and net change (squares). Data show mean values and standard errors (n = 8). The three periods are: period 1: 25 May – 24 July 2023, period 2: 25 July – 11 September 2023 and period 3: 12 September – 30 October 2023. Note the different scales on vertical axes in A) and B).

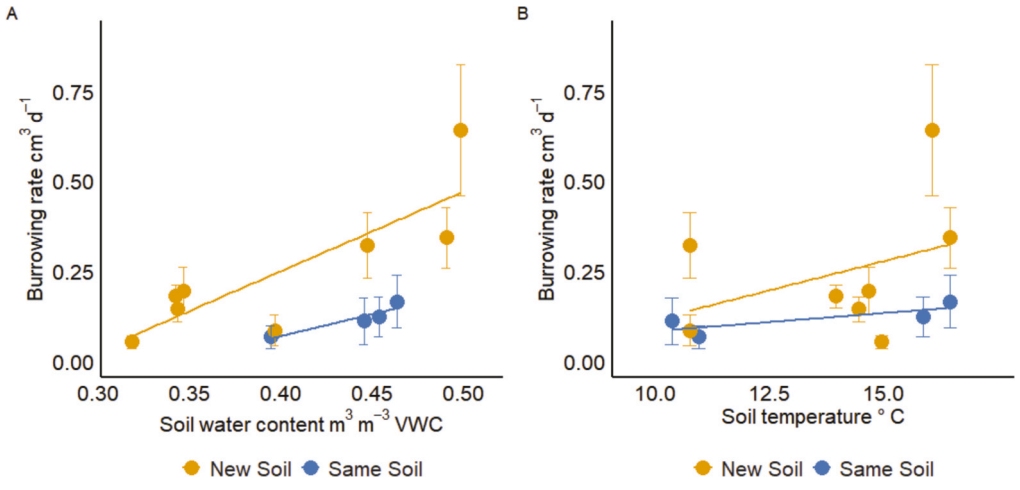

Fig. 5. Burrowing rate as a function of A) soil water content and B) soil temperature, for cylinders with repacked new soil after each scan (orange) and cylinders where the same soil with intact burrow networks were reinstalled in the field after each scan (blue). Note: because initial conditions (repacked soil) were the same for all cylinders at initial installation, there are eight data points for "new soil"(corresponding to the first period in all treatments and the second and third period of the "new soil treatment") and only four data points (corresponding to the second and third period of the "same soil treatment").

"same soil" columns slightly decreased over time (Fig. 4). The rate of net change in burrow volume (i.e., difference between created and disappearing burrows) approached a value close to zero in period 3 for the "same soil" columns (Fig. 4, right), which might indicate convergence towards a steady-state burrow volume (i.e., created and disappearing burrow volumes are in balance). The mean burrowing rates were significantly lower ($p < 0.001$) in the "same soil" than the "new soil" treatment. See supplementary fig. 6 for the relation between the columns with new soil and the same soil columns.

Mean burrowing rates over the entire study period (25 May – 30 October) were about 1×10^{-4} cm^3 cm^{-3} d^{-1} for the "same soil" columns and approximately 2×10^{-4} cm^3 cm^{-3} d^{-1} for the "new soil" columns. To put this in perspective, these burrowing rates correspond to soil turnover times (i.e. the time it would take for earthworms to burrow the complete volume of topsoil) of about 42 and 21 years for the "same soil" and "new soil" treatments, respectively, assuming that the earthworm community is active from mid-April to mid-November (and inactive for the rest of the year, because of cold temperatures).

We aimed to have two soil moisture treatments (with and without rainout shelters), however, based on the soil moisture sensor data (Supplementary Fig. S3) we did not achieve differences in soil water content between treatments except for period 3 (11 September – 30 October) where the mean volumetric soil water content was 0.44 m^3 m^{-3} in the treatment without rainout shelters and 0.38 m^3 m^{-3} in the treatment with shelters. Nevertheless, soil water contents as well as soil temperature differed between periods, and hence we could relate soil conditions to burrowing rates. Burrowing rates significantly ($p < 0.001$) increased with increasing soil water content (Fig. 5a), while there was no significant ($p = 0.82$) increase in burrowing rates with soil temperature (Fig. 5b). We acknowledge that the relationships between burrowing rates and soil water content and temperature, respectively, are uncertain due to the limited number of data points.

Burrow volumes slightly decreased with depth (Fig. 6). The depth above and below which 50% of the total burrow volume were located was between 4.5 and 8.5 cm, corresponding to 9.5 and 13.5 cm soil depth (cylinders were installed 5 cm below soil surface), with no clear temporal pattern and little differences between treatments (Supplementary Fig. S7). The size distribution of earthworm burrows showed no clear temporal pattern (Fig. 6D.). There were only a few burrows with a diameter larger than 6 mm.

3.2. Burrow networks created by anecic and endogeic earthworms

Based on both samplings, we measured an earthworm biomass of 35 g per m^2, an earthworm abundance of 81 individuals per m^2 and identified five different earthworm species (Supplementary Table S2): *Aporrectodea rosea, Aporrectodea caliginosa, Aporrectodea tuberculata, Aporrectodea longa* and *Lumbricus terrestris*. *A. rosea*, *A. caliginosa* and *A. tuberculata* are predominantly endogeic species (Bottinelli et al. 2020), while *A. longa* and *L. terrestris* are mainly anecic (Bottinelli et al.

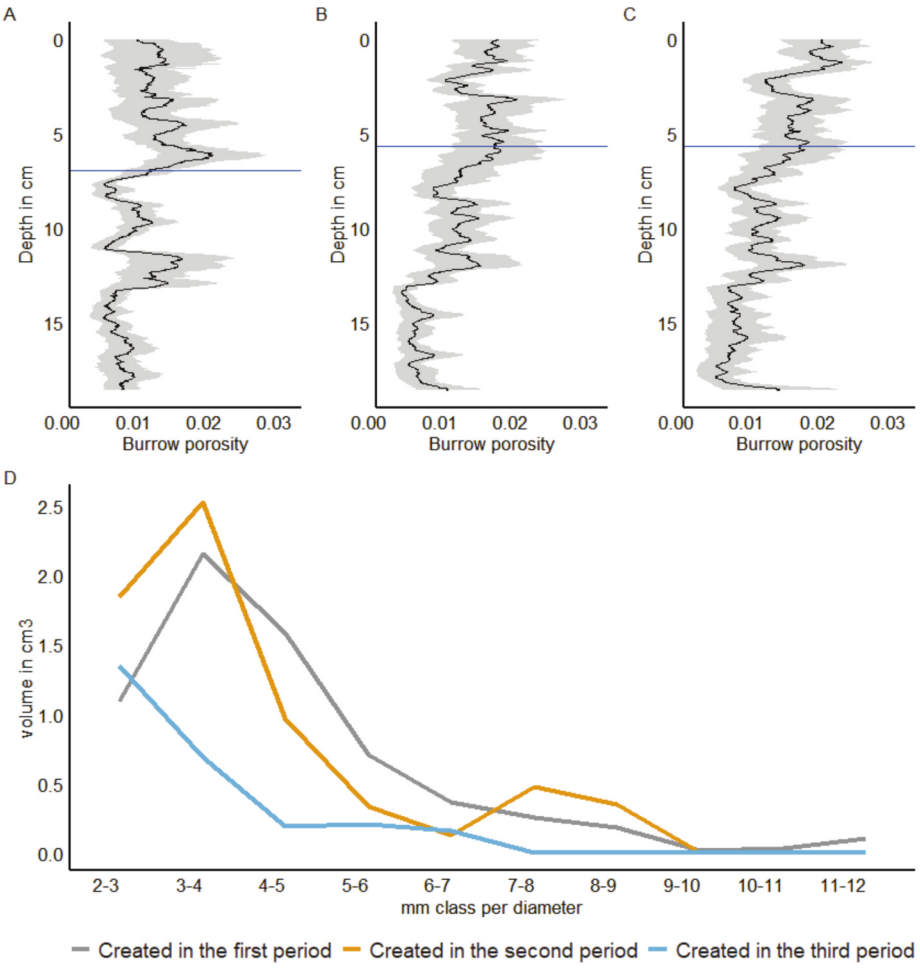

Fig. 6. Depth distribution of burrow volume, from the treatment combination "same soil with rainout shelters", for Period 1 (A), Period 2 (B) and Period 3 (C). The blue line indicates the point where 50% of the burrow volume is above and below. The grey area around the line indicates the standard error. The other treatments showed a similar depth distribution trend (Supplementary Fig. S10). The diameter distribution for the burrows created in each class for each period is shown in (D). The three periods are: period 1: 25 May – 24 July 2023, period 2: 25 July – 11 September 2023 and period 3: 12 September – 30 October 2023.

2020). Individuals of *A. rosea*, *A. caliginosa* and *A. tuberculata* weighed around 0.3 g, while individuals of *A. longa* and *L. terrestris* had a fresh body weight of 1.5–3 g (Supplementary Table S2).

Fig. 7 shows an earthworm burrow network (Fig. 7C), and its separation into burrows likely created by anecic earthworms (>4 mm; Fig. 7B) and endogeic earthworms (≤4 mm; Fig. 7A). The volume fraction of endogeic burrows across all soil cylinders varied between 0.4 and 0.8, and no temporal pattern across the three periods from May to October 2023 could be revealed. On average across all columns and periods, the total burrow volume was comprised of roughly 60% endogeic burrows and 40% anecic burrows.

Endogeic burrows were significantly less persistent than anecic burrows ($p < 0.001$). Of all endogeic burrow volume, on average 52% disappeared between scans. For anecic burrows, 28% of burrow volume disappeared (see Supplementary Fig. S8 for details). No significant difference ($p = 0.74$) in the orientation of burrows between endogeic (angle of orientation: 52°) and anecic burrows (angle of orientation: 51°) was found. Endogeic burrows had an average tortuosity of 1.52 and were significantly more tortuous ($p = 0.032$) than anecic burrows (mean tortuosity of 1.37). There were more ($p < 0.001$) endogeic burrow clusters (number of clusters per column: 23.4) than anecic burrow clusters (number of clusters per column: 7.8). There were no significant differences between endogeic and anecic burrows for coordination number ($p = 0.06$) and branching intensity ($p = 0.62$).

4. Discussion

4.1. Bi-monthly scanning of soil columns to monitor earthworm burrow networks

One of our aims was to develop and test a method for monitoring field earthworm burrowing rates. Our study demonstrates that this is feasible using perforated cylinders that are temporarily extracted from the field for X-ray imaging. The holes of 11 mm in diameter allowed earthworms, even large anecic individuals, to enter and leave soil cores from all sides. While repeated X-ray scanning of soil columns installed under field conditions to monitor changes in soil structure has been done in earlier studies (Koestel & Schlüter 2019), only a few (Leuther et al., 2023; Schefer et al., 2025; Védère et al., 2025) have utilized perforated walls to allow macrofauna and roots to freely enter and leave the soil columns. To the best of our knowledge, we present the first study to quantify earthworm burrowing rates at intervals of about two months. Védère et al. (2025) incubated soil cores in perforated cylinders for one year and then quantified macrofaunal pore networks. They did their study at several sites around the world and linked biopore characteristics to specific macrofauna (e.g. earthworms). The studies of Schefer et al. (2025) and Leuther et al. (2023) both showed the development in soil structure and the macropore changes over a long-term period of 6–24 months. To better capture temporal dynamics in biopores, Védère et al. (2025) suggested scanning at shorter time intervals, which we employed in our study. Leuther et al. (2023) estimated soil structure turnover rates and concluded that macrofaunal activity was a primary driver of soil structure dynamics but did not explicitly quantify earthworm burrowing rates. Koestel and Schlüter (2019) used a soil column that was open on the top and bottom but had solid walls that did not allow lateral movement of macrofauna. They mentioned the formation of biopores by earthworms as an important driver of soil structure dynamics but did not quantify the relative contribution of earthworms to changes in macroporosity. Leuther et al. (2023) scanned their soil column every six months, while we scanned at intervals of about two months. The shorter time interval between scans allows for a better link between soil environmental conditions and changes in soil macropore structure.

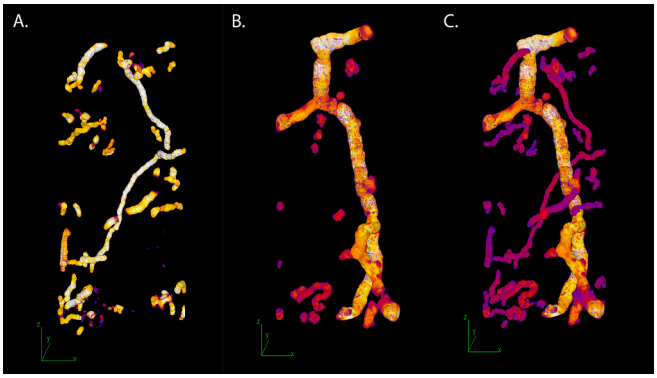

Fig. 7. Illustrative example of soil column showing earthworm burrows likely created by endogeic earthworms (A) and anecic earthworms (B), and the total earthworm burrow network (C). Burrows ≤ 4 mm were classified as "endogeic burrows" and burrows > 4 mm as "anecic burrows". The colour scale of the burrows indicates the relative burrow diameter, where white is the largest and purple the smallest diameter. Note that this is a relative scale for each image.

We compared two methodological approaches, namely, to re-install the same soil column after each scan and to use a soil column repacked with new soil after each scan. Using the same soil after each scan, which might represent more realistic "natural" conditions, allows the identification of newly created burrows and the destruction of burrows and to quantify the persistence of earthworm burrows, but requires alignment of the images at each scan time, and the quantifications are sensitive to distortions of the cylinders and shrinking or swelling of the soil. Using soil columns repacked with new soil after each scan makes the quantification of newly formed burrows easier and there are no requirements for image registration but does not allow to quantify burrow "turnover" or persistence. Based on our study, using the same soil column seemed advantageous as image registration was not a major obstacle, and based on the alignment of the soil columns, the soil cores did not noticeably deform (e.g. due to shrink-swell processes), but this experience may not be generalizable to other soils or climates. In future studies, we recommend using markers to help facilitate the alignment process.

Burrowing rates were higher in new, repacked soil than in the "same" soil treatment. It remains unclear whether this is because uncolonized soil in the new, repacked soil columns present favourable conditions that attracted earthworms or whether earthworms are reluctant to enter already colonized soil with burrows in the "same" soil treatment. Capowiez & Belzunces (2001) showed, using 2D terraria, that anecic earthworms avoided already occupied burrows whereas this was not the case for endogeic earthworms. The soil columns repacked with new soil may represent a similar disturbance as soil tillage, after which earthworms can restructure the soil. We speculate that new, remoulded, "fresh" soil may indicate a potential maximum burrowing rate under given soil moisture and temperature conditions, but this would need to be tested in future studies. In contrast, repeated imaging of the same soil provides information on the duration until a steady-state burrow structure is reached (e.g. after a disturbance). Our data indicates that a steady-state (i.e., a balance between newly created and disappearing burrows) might be reached at the end of the five-months study period (Fig. 4b). Védère et al. (2025) incubated soil cores for one year and found that biopores regenerate within a year at most sites.

More frequent scans or a longer total observation period than in our study would be needed and to establish robust relationships between burrowing rates and soil environmental conditions. It would have been interesting to quantify earthworm casts within the cylinders, as this would have allowed a comparison with findings by Capowiez et al. (2014), who reported that 40–50% of the burrow volume created by endogeic earthworms was filled with casts, compared to only about 20% for anecic earthworms. However, a density difference between the earthworm casts and surrounding soil matrix could not be discerned, and as a result, it was not possible to identify casts on our images. This may also have resulted in an underestimation of burrow volumes. Hence, although we quantified the volume of burrows that disappeared

between successive scans, we were unable to determine the mechanisms behind this disappearance, i.e. whether burrows collapsed or were filled by casts.

4.2. Temporal dynamics of earthworm burrow systems and burrowing rates

Burrowing rates increased from July to September and slightly decreased in the last period from mid-September to October for the soil columns with the new soil. In the soil columns with the same soil, the burrowing rates slightly decreased over time from May to October. Based on the analysis of the depth distribution, the depth at which 50% of the burrow volume is above and below, respectively, was located at a slightly deeper point in the soil during the first period than during the remainder of the time (Supplementary Fig. S7). This difference might be explained by drier soil conditions during the first period. We found that burrowing rates increased with increasing soil moisture, whereas soil temperature appeared to be a weaker driver. Gergs et al. (2022) found similar results, where earthworm activity increased when the soil moisture content increased.

Studies under controlled conditions have shown that soil moisture and soil temperature influence earthworm activity and development. A higher soil moisture content and higher soil temperature can result in higher earthworm growth rates and faster development of earthworms (Wever et al. 2001; Taylor et al. 2019), which is expected to increase annual earthworm bioturbation (Taylor et al. 2019; Torppa & Taylor 2022). Burrowing activity and surface casting have been shown to increase with an increase in temperature. For example, burrow length was found to be between 40–80% shorter at 5 °C than at 15 °C (Perreault & Whalen 2006). Soil moisture and soil temperature control whether earthworms are active or in aestivation, and this response is species dependent. For example, *Aporrectodea caliginosa* enters aestivation in winter due to low temperatures and in summer due to dry soil conditions, while e.g. *Lumbricus terrestris* seems less temperature sensitive and its activity is primarily controlled by soil moisture (Nordström & Nordstrom 1975; Andriuzzi et al. 2015; Potvin & Lilleskov 2017). We identified earthworms in aestivation in some of the soil columns during the first imaging at the end of a dry period (Supplementary Fig. S2), and this would explain the reduced burrowing rates during the first period. No earthworms in aestivation were identified during periods two and three.

Knowledge on earthworm bioturbation and burrowing rates under field conditions is limited. Leuther et al. (2023), using a similar approach as in our study, demonstrated that macrofauna and especially earthworm burrowing is an essential driver of topsoil structure turnover. They estimated topsoil structure turnover times of 16 years in a Luvisol (mean annual precipitation about 500 mm) and 33 years in a Chernozem (mean annual precipitation about 900 mm) when soil biota had access to their samples, and concluded that the difference between the sites was probably due to differences in soil moisture. Based on our data covering a period from the end of May until the end of October, the estimated average earthworm burrow rates suggest that the whole topsoil volume would be burrowed in about 12–24 years (depending on treatments), i.e. a "turnover time" of the topsoil of one to two decades. These estimates do not consider the potential inactivity of earthworms during winter or activity patterns during spring – further studies that cover a whole year (or more) are therefore needed. If we consider that earthworms are only active from mid-April to mid-November, when the soil is warm enough for earthworms to be active, the estimated "burrowing turnover times" would be 21–42 years. These figures are uncertain but give an indication of how long it would take for earthworms to process the whole topsoil. We note that burrowing rates obtained in 2D-terraria are higher (e.g. Arrázola-Vásquez et al., 2022), which is likely because these are short-term studies with more favourable soil conditions for burrowing compared with field conditions of our study.

4.3. Identification of earthworm burrow systems created by anecic and endogeic earthworms

In this study, we found a threshold of 4 mm suitable to separate "anecic" burrows (>4 mm in diameter) from "endogeic" burrows (<4 mm in diameter). This separation using diameter is feasible for adults. It is known that juveniles of anecic species tend to behave more like endogeic species. Hence, young anecic earthworms with a diameter of < 4 mm would be classified as endogeic by our method, which however reflects their burrowing behaviour. Visual inspection (e.g. Fig. 6) and quantification of the 3D burrow networks reveal that burrows likely created by anecic earthworms were relatively straight (i.e., low tortuosity), as was also found in other studies (Capowiez et al. 2001; 2011; 2015). Tortuosity values calculated in our study are likely underestimations of the tortuosity of the burrowing path due to casting and collapsing of burrows (Supplementary Fig. S9). Since anecic burrows were more stable, the tortuosity should have been larger for the endogeic burrows. Endogeic earthworms created more clusters or separate burrows, which agrees with earlier studies (Capowiez et al. 2015).

Although the earthworm community of our field site included many more endogeic than anecic individuals (Supplementary Table S2) and although there were many more "endogeic burrows" than "anecic burrows", the volume fraction of anecic burrows was around 40% on average. There was likely a larger number of endogeic earthworms entering the columns compared to anecic earthworms. Using our method, we could not assign burrows to earthworms at the species level, nor determine whether the species composition within the columns matched that of the surrounding soil. According to our analysis, burrows created by anecic earthworms had a higher persistency (fraction of burrows disappearing between scans = 0.28) than endogeic burrows (fraction of burrows disappearing between scans = 0.52). More frequent burrow quantification over the course of a year could provide additional information on the persistency of burrows. The features of "anecic burrows" (i.e., low tortuosity, high volume fraction despite low number of burrows, temporal stability) have major implications for soil functioning. Vertically stable macropores connected to the soil surface facilitate water infiltration, soil aeration and gas exchange between soil and atmosphere. Especially under saturated conditions, water mainly flows through earthworm burrows, where connectivity to the soil surface and continuous burrows are highly impacting this flow (Francis & Fraser 1998). Moreover, plant roots can use such burrows to reach resources in deeper soil layers or bypass compacted layers (e.g. plough pans).

Future research could evaluate how many "anecic burrows" and how many anecic earthworms, respectively, are required for optimal soil functioning, or whether there is an optimum ratio of "anecic burrows" to "endogeic burrows". The ability to identify earthworm burrows created by anecic and endogeic earthworms and to monitor the temporal dynamics of the respective burrow systems offers a way to gain new insights into the ecology of anecic and endogeic earthworm species and their roles as soil ecosystem engineers.

5. Conclusion

Monitoring earthworm burrowing rates in the field using perforated cylinders, where earthworms can move in and out, and X-ray scanning the soil columns at regular intervals, was found to be a feasible method. Soil columns with the "same" soil revealed more information on the development of the pore network system, as it was possible to quantify newly created and disappearing burrows. Soil columns that were repacked with new soil after each scan may be suitable to measure maximum burrowing rates in field soil. Data from the "same soil" treatment suggest that a steady state in earthworm burrow volume was obtained after five months, indicated by a balance between burrow creation and disappearance. Based on burrow diameter, we could distinguish between burrows likely created by endogeic earthworms

(burrow diameter ≤ 4 mm) and anecic earthworms (burrow diameter > 4 mm), and this could provide new insights into the burrowing behaviour of these earthworm classes. The fraction by volume of burrows created by endogeic earthworms was approximately 60%, and consequently that by anecic earthworms approximately 40%. The anecic burrows were more persistent over time than the endogeic burrows. Quantification of burrows by earthworm communities helps to better understand and simulate their function in soil ecosystems.

The method presented in this study to assess burrowing rates of an earthworm community in the field rather than of specific species and individual earthworms in closed cylinders has given us the opportunity to get a better understanding of the burrowing activity in a soil under field conditions. Further studies could help connect burrowing activity to soil functioning. Higher temporal resolution could help to link environmental conditions to burrowing rates. Monitoring a whole year including winter is required to delineate conditions limiting earthworm burrowing activity.

CRediT authorship contribution statement

Rebecca Naomi ter Borg: Writing – original draft, Visualization, Methodology, Investigation, Formal analysis, Data curation, Conceptualization. **Mats Larsbo:** Writing – review & editing, Supervision, Methodology, Funding acquisition, Formal analysis, Conceptualization. **Yvan Capowiez:** Writing – review & editing, Conceptualization. **Pascal Benard:** Writing – review & editing, Formal analysis. **Astrid Taylor:** Writing – review & editing. **Daniel Iseskog:** Methodology. **Thomas Keller:** Writing – review & editing, Project administration, Methodology, Funding acquisition, Conceptualization.

Declaration of competing interest

The authors declare that they have no known competing financial interests or personal relationships that could have appeared to influence the work reported in this paper.

Acknowledgements

This research was funded by Formas (grant no 2021-00966). We would like to thank everyone who helped in both the field and the laboratories. We thank Jesper Rydén from the department of Energy and Technology at SLU for the statistical help. For the help with the earthworm identification, we would like to thank Mila Skoglund from the department of Ecology at SLU.

Appendix A. Supplementary data

Supplementary data to this article can be found online at https://doi.org/10.1016/j.geoderma.2026.117838.

Data availability

The data are available from the authors upon request.

References

Andriuzzi, W.S., Pulleman, M.M., Schmidt, O., Faber, J.H., Brussaard, L., 2015. Anecic earthworms (Lumbricus terrestris) alleviate negative effects of extreme rainfall events on soil and plants in field mesocosms. Plant and Soil 397 (1–2), 103–113. https://doi.org/10.1007/s11104-015-2604-4.

Arganda-Carreras, I., Fernández-González, R., Muñoz-Barrutia, A., Ortiz-De-Solorzano, C., 2010. 3D reconstruction of histological sections: Application to mammary gland tissue. Microsc. Res. Tech. 73 (11), 1019–1029. https://doi.org/10.1002/jemt.20829.

Arrázola-Vásquez, Elsa, M., Mats Larsbo, Yvan, Capowiez., Astrid, Taylor., Anke, M. Herrmann., Thomas, Keller., 2024. Estimating Energy Costs of Earthworm Burrowing Using Calorimetry. European Journal of Soil Biology 121, 103619. https://doi.org/10.1016/j.ejsobi.2024.103619.

Arrázola-Vásquez, E., Larsbo, M., Capowiez, Y., Taylor, A., Sandin, M., Iseskog, D., Keller, T., 2022. Earthworm burrowing modes and rates depend on earthworm species and soil mechanical resistance. Appl. Soil Ecol. 178, 104568. https://doi.org/10.1016/j.apsoil.2022.104568.

Baker, G.H., Whitby, W.A., 2003. Soil pH preferences and the influences of soil type and temperature on the survival and growth of Aporrectodea longa (Lumbricidae). Pedobiologia 47 (5–6), 745–753. https://doi.org/10.1078/0031-4056-00254.

Bardgett, R.D., van der Putten, W.H., 2014. Belowground biodiversity and ecosystem functioning. Nature 515 (7528), 505–511. https://doi.org/10.1038/nature13855.

Barot, S., Blouin, M., Fontaine, S., Jouquet, P., Lata, J.-C. & Mathieu, J. (2007). A Tale of Four Stories: Soil Ecology, Theory, Evolution and the Publication System. Rantalainen, M.-L. (red.) (Rantalainen, M.-L., red.) *PLoS ONE*, 2 (11), e1248. https://doi.org/10.1371/journal.pone.0001248.

Blouin, M., Hodson, M.E., Delgado, E.A., Baker, G., Brussaard, L., Butt, K.R., Dai, J., Dendooven, L., Peres, G., Tondoh, J.E., Cluzeau, D., Brun, J.-J., 2013. A review of earthworm impact on soil function and ecosystem services. Eur. J. Soil Sci. 64 (2), 161–182. https://doi.org/10.1111/ejss.12025.

Bottinelli, N., Hedde, M., Jouquet, P., Capowiez, Y., 2020. An explicit definition of earthworm ecological categories – Marcel Bouché's triangle revisited. Geoderma 372, 114361. https://doi.org/10.1016/j.geoderma.2020.114361.

Bouché, M.B., 1977. Strategies lombriciennes. Ecol. Bull. 25, 122–132.

Capowiez, Y., Belzunces, L., 2001. Dynamic study of the burrowing behaviour of Aporrectodea nocturna and Allolobophora chlorotica: interactions between earthworms and spatial avoidance of burrows. Biol. Fertil. Soils 33 (4), 310–316. https://doi.org/10.1007/s003740000327.

Capowiez, Y., Bottinelli, N., Sammartino, S., Michel, E., Jouquet, P., 2015. Morphological and functional characterisation of the burrow systems of six earthworm species (Lumbricidae). Biol. Fertil. Soils 51 (7), 869–877. https://doi.org/10.1007/s00374-015-1036-x.

Capowiez, Y., Marchán, D., Decaëns, T., Hedde, M., Bottinelli, N., 2024. Let earthworms be functional - Definition of new functional groups based on their bioturbation behavior. Soil Biol. Biochem. 188, 109209. https://doi.org/10.1016/j.soilbio.2023.109209.

Capowiez, Y., Monestiez, P., Belzunces, L., 2001. Burrow systems made by Aporrectodea nocturna and Allolobophora chlorotica in artificial cores: morphological differences and effects of interspecific interactions. Appl. Soil Ecol. 16 (2), 109–120. https://doi.org/10.1016/S0929-1393(00)00110-4.

Capowiez, Yvan, Nicolas, Bottinelli, Pascal, Jouquet, 2014. Quantitative Estimates of Burrow Construction and Destruction, by Anecic and Endogeic Earthworms in Repacked Soil Cores. Applied Soil Ecology 74, 46–50. https://doi.org/10.1016/j.apsoil.2013.09.009.

Capowiez, Y., Sammartino, S., Keller, T., Bottinelli, N., 2021. Decreased burrowing activity of endogeic earthworms and effects on water infiltration in response to an increase in soil bulk density. Pedobiologia 85–86, 150728. https://doi.org/10.1016/j.pedobi.2021.150728.

Capowiez, Y., Sammartino, S., Michel, E., 2011. Using X-ray tomography to quantify earthworm bioturbation non-destructively in repacked soil cores. Geoderma 162 (1), 124–131. https://doi.org/10.1016/j.geoderma.2011.01.011.

Darwin, C. (1881). *The formation of vegetable mould, through the action of worms, with observations on their habits.* https://babel.hathitrust.org/cgi/pt?id=nyp.33433007858008&seq=17 [2023-12-06].

Dittbrenner, N., Moser, I., Triebskorn, R., Capowiez, Y., 2011. Assessment of short and long-term effects of imidacloprid on the burrowing behaviour of two earthworm species (Aporrectodea caliginosa and Lumbricus terrestris) by using 2D and 3D post-exposure techniques. Chemosphere 84 (10), 1349–1355. https://doi.org/10.1016/j.chemosphere.2011.05.011.

Dougherty, R., Kunzelmann, K.-H., 2007. Computing Local Thickness of 3D Structures with ImageJ. Microsc. Microanal. 13 (S02). https://doi.org/10.1017/S1431927607074430.

P. Dunn Tweedie: Evaluation of Tweedie Exponential Family Models 2022 24.

C.A. Edwards N.Q. Arancon Biology and ecology of earthworms Fourth edition 2022 Springer.

Eggleton, P., Inward, K., Smith, J., Jones, D.T., Sherlock, E., 2009. A six year study of earthworm (Lumbricidae) populations in pasture woodland in southern England shows their responses to soil temperature and soil moisture. Soil Biol. Biochem. 41 (9), 1857–1865. https://doi.org/10.1016/j.soilbio.2009.06.007.

Francis, G.S., Fraser, P.M., 1998. The effects of three earthworm species on soil macroporosity and hydraulic conductivity. Appl. Soil Ecol. 10 (1), 11–19. https://doi.org/10.1016/S0929-1393(98)00045-6.

Garbout, A., Munkholm, L.J., Hansen, S.B., 2013. Tillage effects on topsoil structural quality assessed using X-ray CT, soil cores and visual soil evaluation. Soil Tillage Res. 128, 104–109. https://doi.org/10.1016/j.still.2012.11.003.

Gergs, A., Rakel, K., Bussen, D., Capowiez, Y., Ernst, G., Roeben, V., 2022. Integrating earthworm movement and life history through dynamic energy budgets. Conservation Physiology 10 (1), coac042. https://doi.org/10.1093/conphys/coac042.

Heinze, W.M., Mitrano, D.M., Lahive, E., Koestel, J., Cornelis, G., 2021. Nanoplastic Transport in Soil via Bioturbation by Lumbricus terrestris. Environ, Sci. Technol., p. 11

Holmstrup, M., Slotsbo, S., Henriksen, P.G., Bayley, M., 2016. Earthworms accumulate alanine in response to drought. Comp. Biochem. Physiol. A Mol. Integr. Physiol. 199, 8–13. https://doi.org/10.1016/j.cbpa.2016.04.015.

Jégou, D., Cluzeau, D., Wolf, H.J., Gandon, Y., Tréhen, P., 1997. Assessment of the burrow system of Lumbricus terrestris, Aporrectodea giardi, and Aporrectodea caliginosa using X-ray computed tomography. Biol. Fertil. Soils 26 (2), 116–121. https://doi.org/10.1007/s003740050353.

Kassambara, A. (2023). *ggpubr: "ggplot2" Based Publication Ready Plots* (R package version 0.6.0). https://CRAN.R-project.org/package=ggpubr.
Koestel, J., 2018. SoilJ: an ImageJ Plugin for the Semiautomatic Processing of Three-Dimensional X-ray Images of Soils. Vadose Zone J. 17 (1), 1–7. https://doi.org/10.2136/vzj2017.03.0062.
Koestel, J., Schlüter, S., 2019. Quantification of the structure evolution in a garden soil over the course of two years. Geoderma 338, 597–609. https://doi.org/10.1016/j.geoderma.2018.12.030.
Lavelle, P., 1988. Earthworm activities and the soil system. Biol. Fertil. Soils 6 (3), 237–251. https://doi.org/10.1007/BF00260820.
Legland, D., Arganda-Carreras, I., Andrey, P., 2016. MorphoLibJ: integrated library and plugins for mathematical morphology with ImageJ. Bioinformatics 32 (22), 3532–3534. https://doi.org/10.1093/bioinformatics/btw413.
Leuther, F., Mikutta, R., Wolff, M., Kaiser, K., Schlüter, S., 2023. Structure turnover times of grassland soils under different moisture regimes. Geoderma 433, 116464. https://doi.org/10.1016/j.geoderma.2023.116464.
Nordstrom, S., Rundgren, S., 1973. Associations of lumbricids in Southern Sweden. Pedobiologia 13 (4), 301–326. https://doi.org/10.1016/S0031-4056(23)02114-5.
Nordström, S., Nordstrom, S., 1975. Seasonal activity of Lumbricids in Southern Sweden. Oikos 26 (3), 307. https://doi.org/10.2307/3543501.
Ollion, J., Cochennec, J., Loll, F., Escudé, C., Boudier, T., 2013. TANGO: a generic tool for high-throughput 3D image analysis for studying nuclear organization. Bioinformatics 29 (14), 1840–1841. https://doi.org/10.1093/bioinformatics/btt276.
Perreault, J.M., Whalen, J.K., 2006. Earthworm burrowing in laboratory microcosms as influenced by soil temperature and moisture. Pedobiologia 50 (5), 397–403. https://doi.org/10.1016/j.pedobi.2006.07.003.
Phillips, H.R.P., Guerra, C.A., Bartz, M.L.C., Briones, M.J.I., Brown, G., Crowther, T.W., Ferlian, O., Gongalsky, K.B., van den Hoogen, J., Krebs, J., Orgiazzi, A., Routh, D., Schwarz, B., Bach, E.M., Bennett, J.M., Brose, U., Decaëns, T., König-Ries, B., Loreau, M., Mathieu, J., Mulder, C., van der Putten, W.H., Ramirez, K.S., Rillig, M.C., Russell, D., Rutgers, M., Thakur, M.P., de Vries, F.T., Wall, D.H., Wardle, D.A., Arai, M., Ayuke, F.O., Baker, G.H., Beauséjour, R., Bedano, J.C., Birkhofer, K., Blanchart, E., Blossey, B., Bolger, T., Bradley, R.L., Callaham, M.A., Capowiez, Y., Caulfield, M.E., Choi, A., Crotty, F.V., Crumsey, J.M., Dávalos, A., Diaz Cosin, D.J., Dominguez, A., Duhour, A.E., van Eekeren, N., Emmerling, C., Falco, L.B., Fernández, R., Fonte, S.J., Fragoso, C., Franco, A.L.C., Fugère, M., Fusilero, A.T., Gholami, S., Gundale, M.J., López, M.G., Hackenberger, D.K., Hernández, L.M., Hishi, T., Holdsworth, A.R., Holmstrup, M., Hopfensperger, K.N., Lwanga, E.H., Huhta, V., Hurisso, T.T., Iannone, B.V., Iordache, M., Joschko, M., Kaneko, N., Kanianska, R., Keith, A.M., Kelly, C.A., Kernecker, M.L., Klaminder, J., Koné, A.W., Kooch, Y., Kukkonen, S.T., Lalthanzara, H., Lammel, D.R., Lebedev, I.M., Li, Y., Jesus Lidon, J.B., Lincoln, N.K., Loss, S.R., Marichal, R., Matula, R., Moos, J.H., Moreno, G., Morón-Ríos, A., Muys, B., Neirynck, J., Norgrove, L., Novo, M., Nuutinen, V., Nuzzo, V., Mujeeb Rahman, P., Pansu, J., Paudel, S., Pérès, G., Pérez-Camacho, L., Piñeiro, R., Ponge, J.-F., Rashid, M.I., Rebollo, S., Rodeiro-Iglesias, J., Rodríguez, M.Á., Roth, A.M., Rousseau, G.X., Rozen, A., Sayad, E., van Schaik, L., Scharenbroch, B.C., Schirrmann, M., Schmidt, O., Schröder, B., Seeber, J., Shashkov, M.P., Singh, J., Smith, S.M., Steinwandter, M., Talavera, J.A., Trigo, D., Tsukamoto, J., de Valença, A.W., Vanek, S.J., Virto, I., Wackett, A.A., Warren, M.W., Wehr, N.H., Whalen, J.K., Wironen, M.B., Wolters, V., Zenkova, I.V., Zhang, W., Cameron, E.K., Eisenhauer, N., 2019. Global distribution of earthworm diversity. Science 366 (6464), 480–485. https://doi.org/10.1126/science.aax4851.
Plaas, E., Meyer-Wolfarth, F., Banse, M., Bengtsson, J., Bergmann, H., Faber, J., Potthoff, M., Runge, T., Schrader, S., Taylor, A., 2019. Towards valuation of biodiversity in agricultural soils: a case for earthworms. Ecol. Econ. 159, 291–300. https://doi.org/10.1016/j.ecolecon.2019.02.003.
Potvin, L.R., Lilleskov, E.A., 2017. Introduced earthworm species exhibited unique patterns of seasonal activity and vertical distribution, and Lumbricus terrestris burrows remained usable for at least 7 years in hardwood and pine stands. Biol. Fertil. Soils 53 (2), 187–198. https://doi.org/10.1007/s00374-016-1173-x.
R Core Team R: a Language and Environment for Statistical Computing. R Foundation for Statistical Computing 2024.
Ruiz, S., Hallett, P., Or, D., 2023. Bioturbation—Physical processes. I: *Reference Module in Earth Systems and Environmental Sciences*. Elsevier B9780128229743001804. https://doi.org/10.1016/B978-0-12-822974-3.00180-4.
Ruiz, S., Or, D., Schymanski, S.J., 2015. Soil Penetration by Earthworms and Plant Roots—Mechanical Energetics of Bioturbation of Compacted Soils. PLoS One 10 (6), e0128914. https://doi.org/10.1371/journal.pone.0128914.
Ruiz, S.A., Bickel, S., Or, D., 2021. Global earthworm distribution and activity windows based on soil hydromechanical constraints. Commun. Biol. 4 (1), 612. https://doi.org/10.1038/s42003-021-02139-5.
Ruiz, S.A., Or, D., 2018. Biomechanical limits to soil penetration by earthworms: direct measurements of hydroskeletal pressures and peristaltic motions. J. R. Soc. Interface 15 (144), 20180127. https://doi.org/10.1098/rsif.2018.0127.
Schefer, R.B., Koestel, J., Mitrano, D.M., 2025. Minimal vertical transport of microplastics in soil over two years with little impact of plastics on soil macropore networks. Commun. Earth Environ. 6 (1), 278. https://doi.org/10.1038/s43247-025-02237-w.
Schindelin, J., Arganda-Carreras, I., Frise, E., Kaynig, V., Longair, M., Pietzsch, T., Preibisch, S., Rueden, C., Saalfeld, S., Schmid, B., Tinevez, J.-Y., White, D.J., Hartenstein, V., Eliceiri, K., Tomancak, P., Cardona, A., 2012. Fiji: an open-source platform for biological-image analysis. Nat. Methods 9 (7), 676–682. https://doi.org/10.1038/nmeth.2019.
Sherlock, E., 2012. *Key to the earthworms of the UK and Ireland*. FSC.
Singh, J., Schädler, M., Demetrio, W., Brown, G.G. & Eisenhauer, N. (2019). Climate change effects on earthworms - a review. *SOIL ORGANISMS*, 91 (3), 113–137. https://doi.org/10.25674/so91iss3pp114.
Taylor, A.R., Lenoir, L., Vegerfors, B., Persson, T., 2019. Ant and Earthworm Bioturbation in Cold-Temperate Ecosystems. Ecosystems 22 (5), 981–994. https://doi.org/10.1007/s10021-018-0317-2.
The MathWorks Inc, 2024. MATLAB Version 24.2.0.2833386, R2024b. https://www.mathworks.com.
Torppa, K.A., Taylor, A.R., 2022. Alternative combinations of tillage practices and crop rotations can foster earthworm density and bioturbation. Appl. Soil Ecol. 175, 104460. https://doi.org/10.1016/j.apsoil.2022.104460.
Védère, C., Boukbida, H.A., Capowiez, Y., Cheik, S., Coulouma, G., Dinh, R.P., Grellier, S., Hammecker, C., Des Tureaux, T.H., Harit, A., Janeau, J.L., Jouquet, P., Maeght, J.L., Podwojewski, P., Rumpel, C., Sammartino, S., Silvera, N., Siltecho, S., Smaili, L., Soulileuth, B., Bottinelli, N., 2025. Macrofaunal biopores: Diversity and regeneration rates across diverse pedoclimatic conditions studied with repacked soil cores. Geoderma 454, 117177. https://doi.org/10.1016/j.geoderma.2025.117177.
Wever, L.A., Lysyk, T.J., Clapperton, M.J., 2001. The influence of soil moisture and temperature on the survival, aestivation, growth and development of juvenile Aporrectodea tuberculata (Eisen) (Lumbricidae). Pedobiologia 45 (2), 121–133. https://doi.org/10.1078/0031-4056-00074.
Wickham, H. (2016). *ggplot2: Elegant Graphics for Data Analysis*. 2nd ed. 2016. Springer International Publishing : Imprint: Springer. (Use R!). https://doi.org/10.1007/978-3-319-24277-4.